iScience, Volume *26*

Supplemental information

Changes in the hydrophobic network of the $FliG_{MC}$ domain induce rotational switching of the flagellar motor

Tatsuro Nishikino, Atsushi Hijikata, Seiji Kojima, Tsuyoshi Shirai, Masatsune Kainosho, Michio Homma, and Yohei Miyanoiri

Supporting Information

This PDF file includes:

Supporting text
Figures S1 to S7
Tables S1 and S2
References

Other supporting materials for this manuscript include the following:

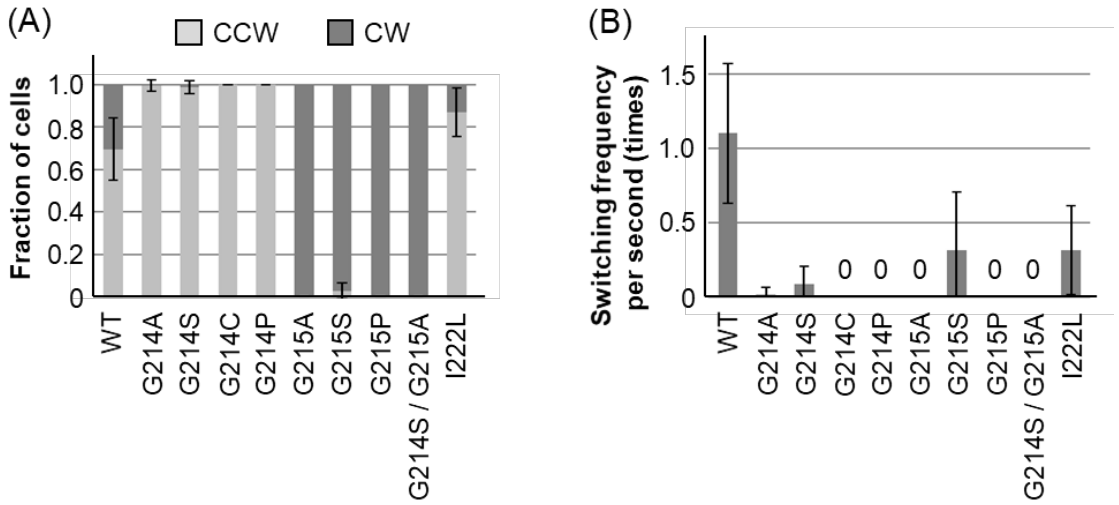

Fig. S1. **Characterization of flagellar rotation with mutations in Gly-Gly flexible linker region, related to Flagellar rotation analysis of FliG mutants (STAR★METHODS).**

The *fliG* mutation (NMB198) harboring pNT1 was grown, and flagellar rotation was observed using high-intensity dark-field microscopy
(A) Counterclockwise rotation (CCW) to clockwise rotation (CW) ratio of *fliG* mutants is shown in light gray and dark gray, respectively. (B) Switching frequency of the cell per second was measured. All experiments were repeated at least six times, and the average values with standard deviation (SD) are shown in the columns.

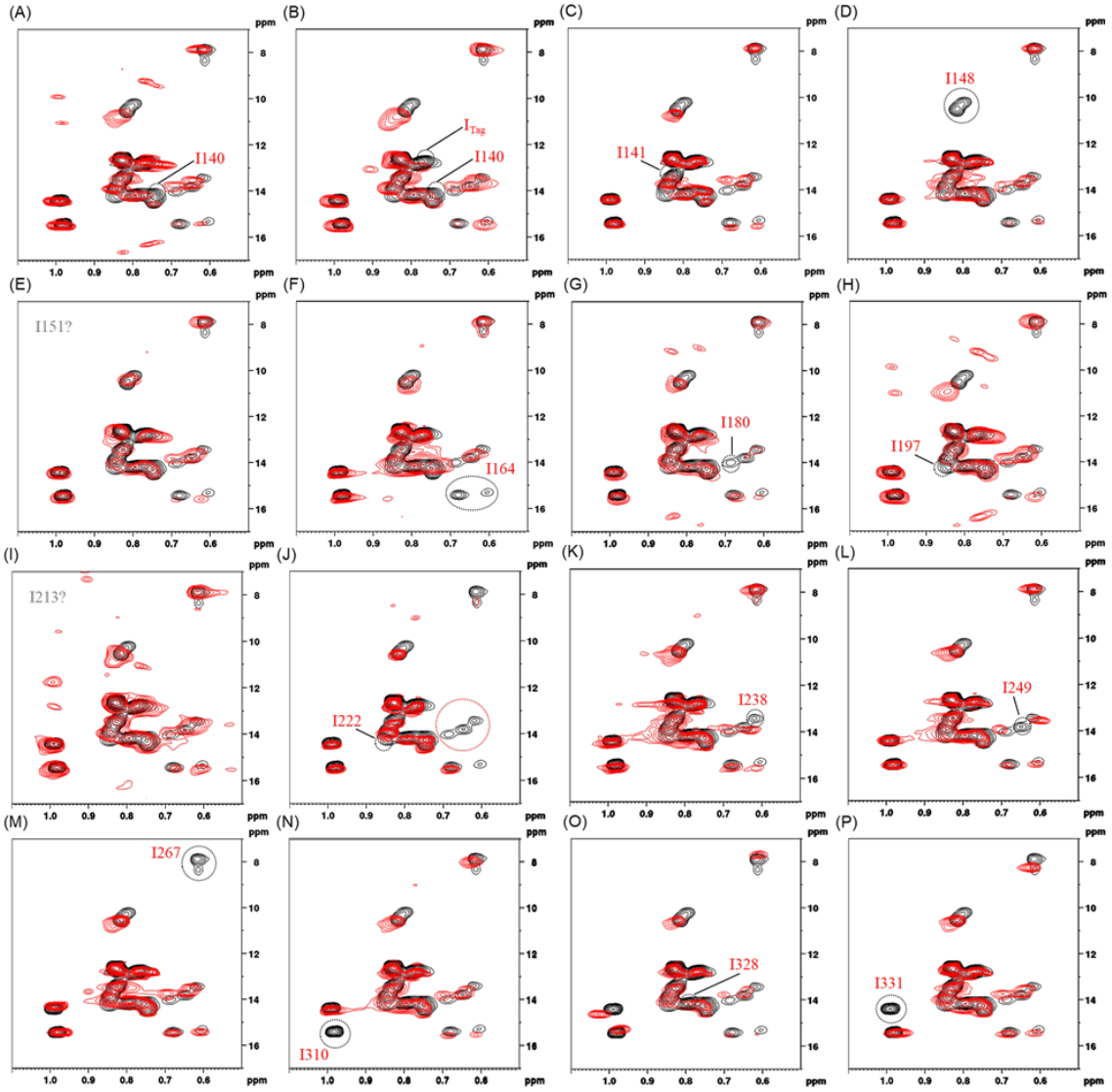

Fig. S2. **Sequence specific assignment of Ile δ1 methyl $^{13}CH_3$ resonances of [δ1-$^{13}CH_3$]-Ile, SAIL-Phe labeled FliG$_{MC}$, related to Figure 2.** The 2D ^{1}H-^{13}C HMQC spectra of labeled mutant FliG$_{MC}$ proteins wherein one of the Ile was replaced by Leu. (A-P) Overlaid ^{1}H-^{13}C HMQC spectrum of labeled WT (black) and mutant FliG(red). The assignment of Ile δ1 resonances are mapped in each spectrum. (A) I140L, (B) I140L without N-terminal Tag, (C) I141L, (D) I148L, (E) I151L, (F) I164L, (G) I180L, (H) I197L, (I) I213L, (J) I222L, (K) I238L, (L) I249L, (M) I267L, (N) I310L, (O) I328L, and (P) I331L.

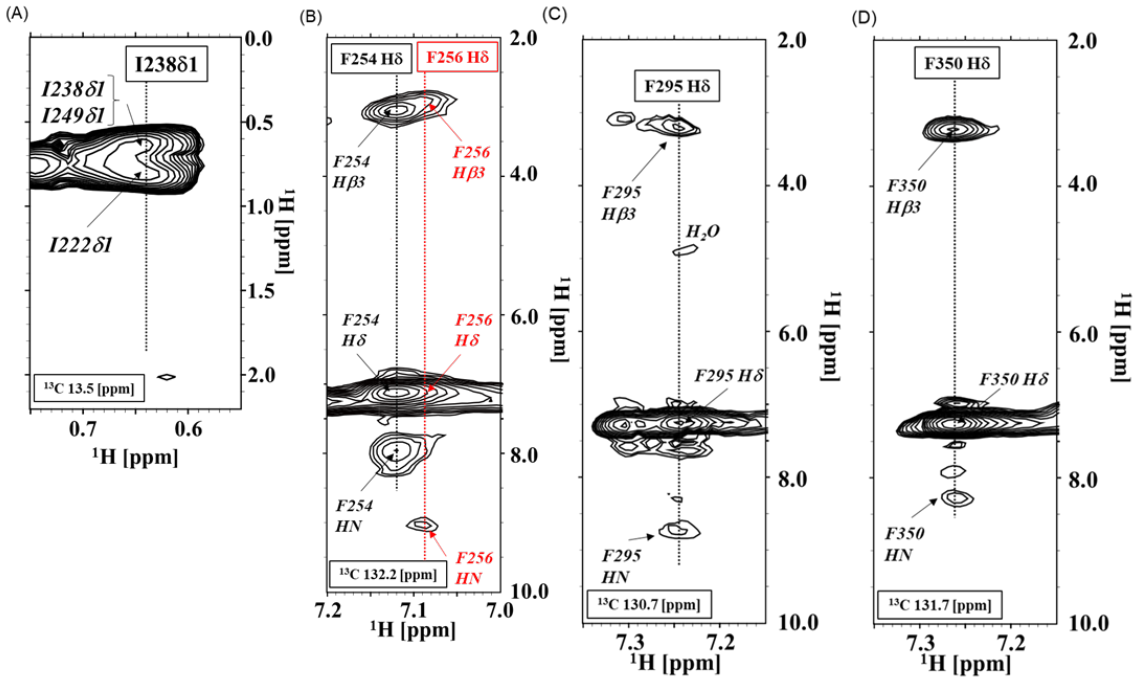

Fig. S3. **Sequence specific assignment of Ile d1 methyl and Phe δ aromatic signals of FliG$_{MC}$ using the NOE analysis, related to Figure 2.** (A) 2D strip of 3D ^{13}C-edited NOESY-HMQC spectrum corresponds to Ile 238 residues in FliG$_{MC}$. From the δ1 methyl signal of Ile 238, the inter-residue NOE signals from Ile 222 and Ile 249 were observed, indicating their spatial proximity.
(B-D) 2D strip of 3D ^{13}C-edited NOESY-TROSY spectrum corresponding to each Phe residues in FliG$_{MC}$, Phe 254, and Phe 256 (B), Phe 295 (C), and Phe 350(D). The intra-residue NOEs between amide (H$_N$), aromatic (H$_δ$), and aliphatic β (H$_{β3}$) signals were observed in each strips.

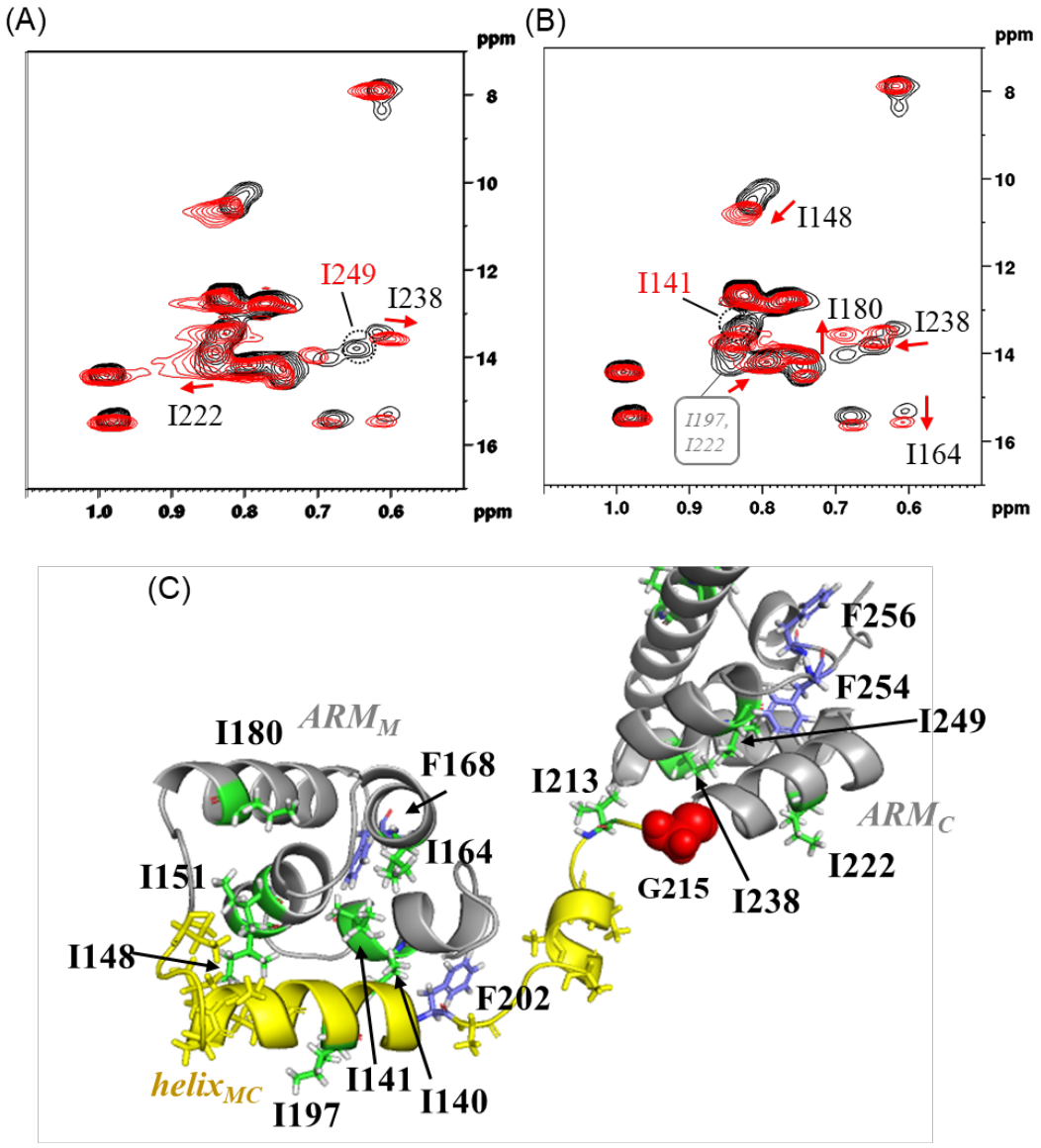

Figure S4. **Hydrophobic interaction networks of FliG$_{MC}$ identified by the chemical shift change induced by single amino acid mutations for the Ile residues, related to Figure 2.** The 2D ^{1}H-^{13}C HMQC spectrum of I249L(A) and I141L(B) mutant (red) was overlaid with that of WT FliG$_{MC}$ (black). The δ1 methyl signal which disappeared in the spectrum for each mutant (dashed circle) was assigned to the Ile residue, which was substituted with Leu residue (red character). The δ1 methyl signal, indicating the secondary chemical shift changes, was attributed to the residues that underwent structural change in presence of the mutation, as indicated by red arrow.

(C) Model structure of $FliG_{MC}$. Ile and Phe residues are indicated as green and blue stick, respectively. The G215 is shown as red sphere. The $helix_{MC}$ domain is shown in yellow, and hydrophobic amino acid residues (i.e. Leu, Val, and Ala) are indicated by yellow stick. As shown in (C) I222, I238, and I249 were located in the ARM_C domain and in close proximity. In the case of I141L mutant, a secondary chemical shift change was observed in several Ile residues (i.e. I148, I164, I180, I197, I222, and I238). Since I141 is located at the interface of ARM_M and $helix_{MC}$, I141L mutation induced secondary chemical shift change to Ile resides in both domains. In addition, it caused secondary chemical shift change in I222 and I238 distal to I141. It is possible that the I141L mutation altered the hydrophobic interaction network between ARM_M and $helix_{MC}$, and its effect were transmitted through hydrophobic residues in $helix_{MC}$ to the ARM_C, thus affecting the chemical shifts of I122 and I238.

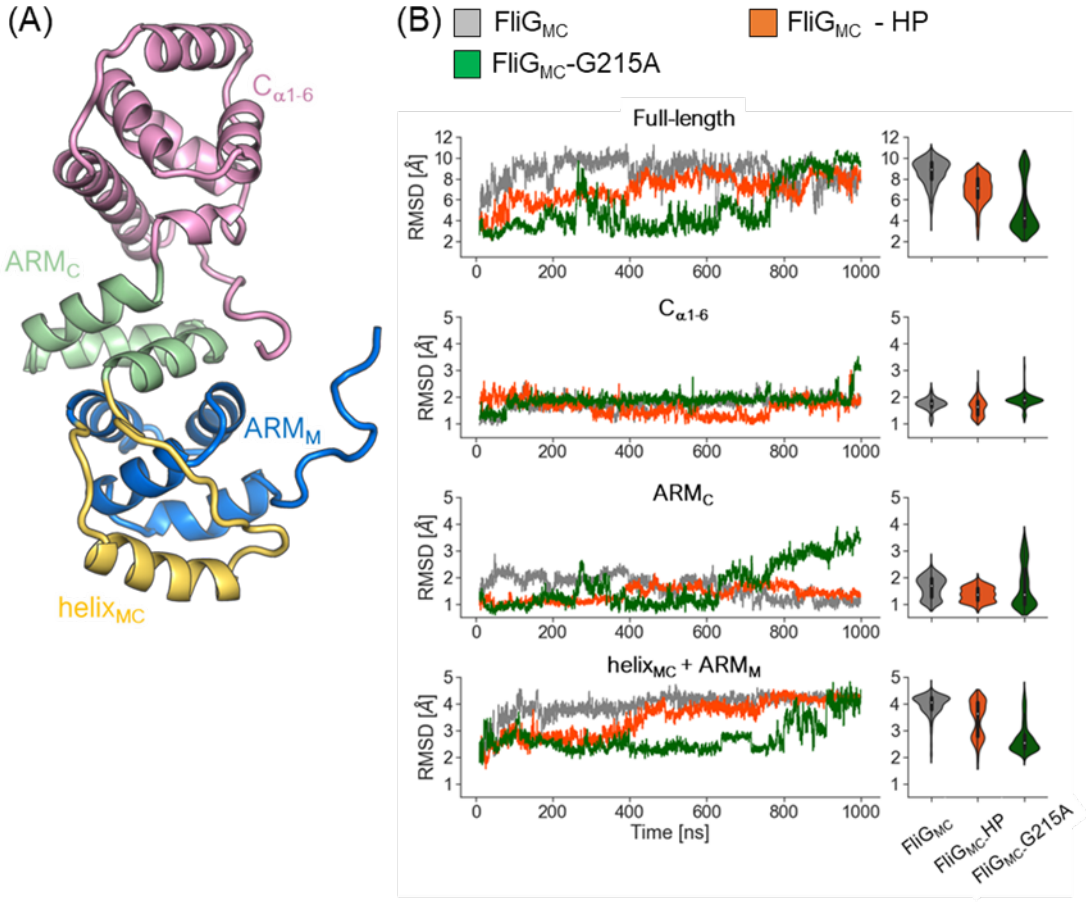

Figure S5. **Structural deviation from initial conformation during the MD simulations, related to Figure 5.** (A) The initial structure of $FliG_{MC}$ fragment model colored by each domain. (B) The root-mean-square deviations (RMSDs) of backbone atoms in the full-length, $C_{\alpha 1\text{-}6}$, ARM_C, and $helix_{MC}$+ARM_M domains from the initial structure during the simulations for $FliG_{MC}$ (gray), $FliG_{MC}$ under 75MPa ($FliG_{MC}$ - HP) (orange) and $FliG_{MC}$-G215A (green), respectively (left panel) and violin-plots of the RMSD distributions for proteins in each condition (right panel).

.(A)

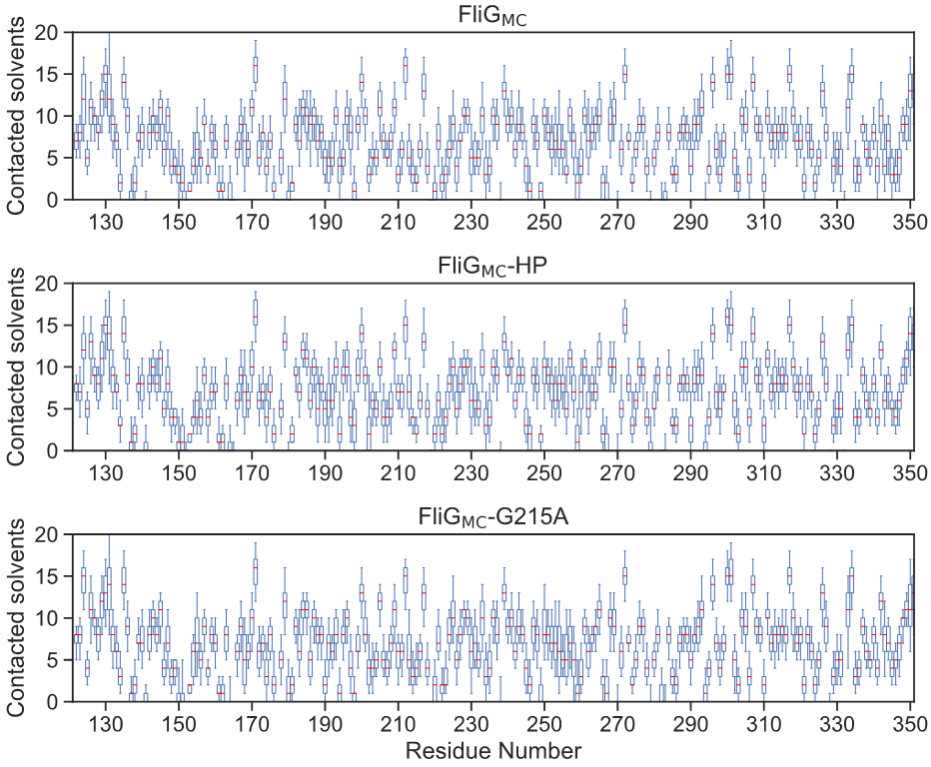

(B)

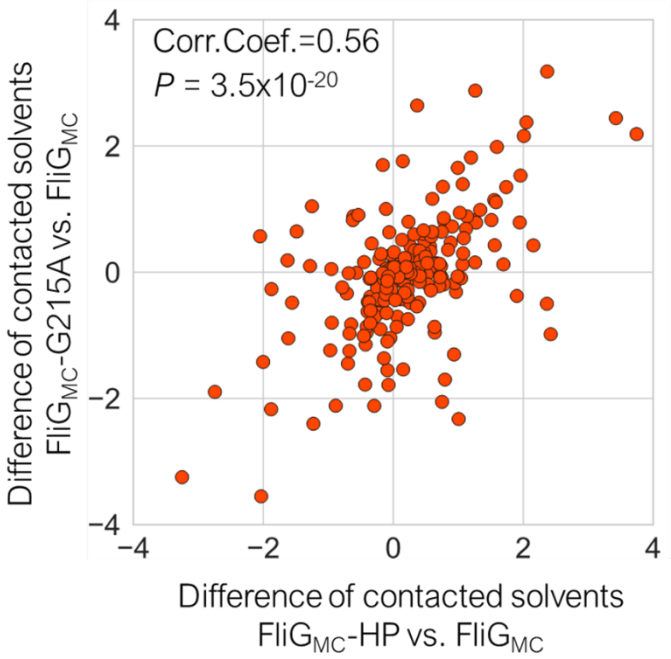

Figure S6. **The number of contacted solvents for each residue of FliG$_{MC}$ and FliG$_{MC}$-G215A, related to Figure 5.** (A) Distribution of the number of contacted solvents for each residue in the 1μs MD simulations. The box plots represent the

distribution of the number of solvents with which each residue contacts in the 2,500 snapshots of the MD trajectories for each protein. The red bars indicate the median values for each residue. The lower and upper whiskers of the plots indicate the 5 and 95 percentiles, respectively. (B) Scatter-plot graph between difference of solvent molecules in contact for $FliG_{MC}$-HP vs. $FliG_{MC}$ and that of $FliG_{MC}$-G215A vs. $FliG_{MC}$. The degrees of change in the solvent accessibility showed a similar trend (Pearson's correlation coefficient: 0.56, P-value = 3.5×10^{-20}).

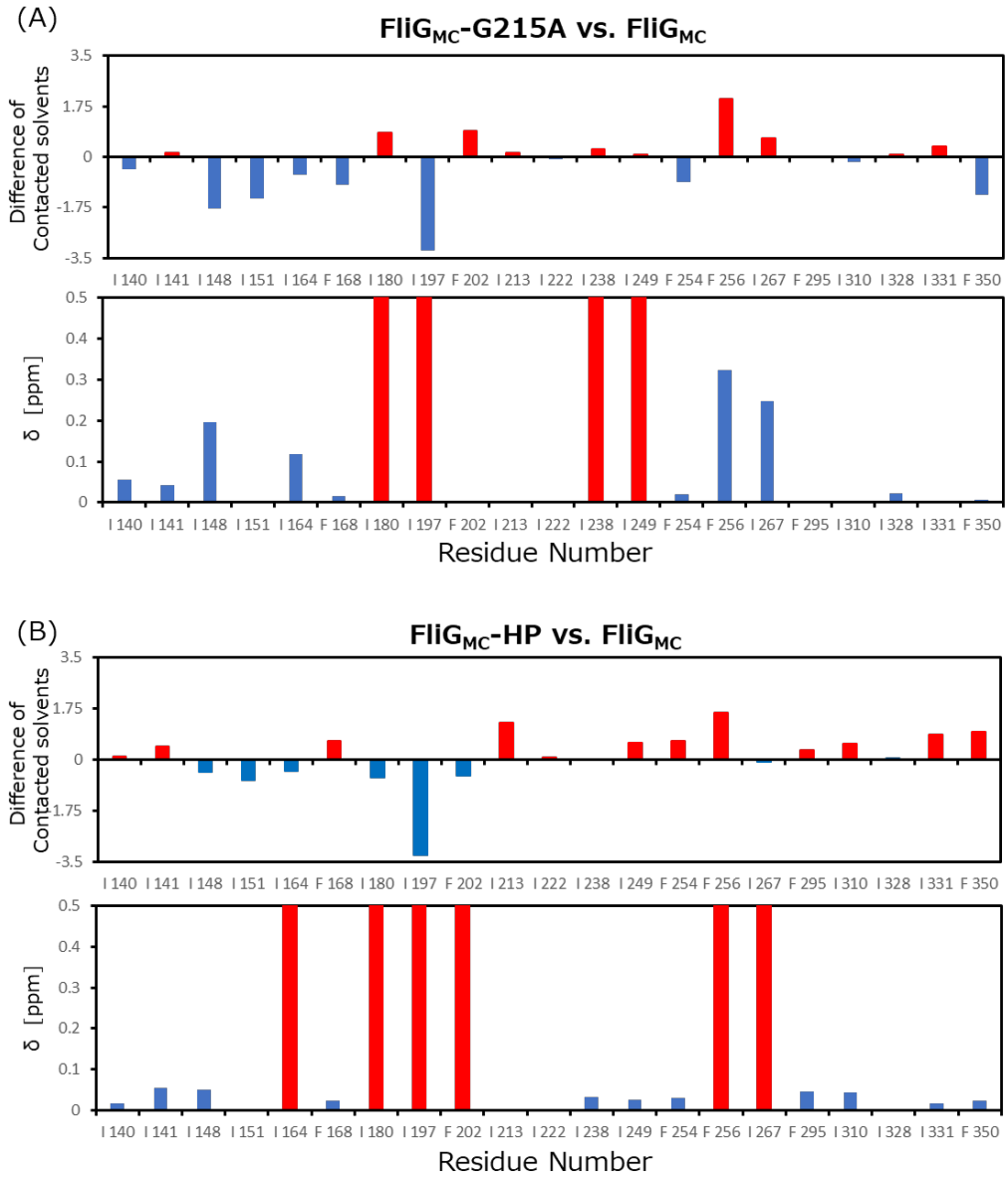

Figure S7. Difference of contacted solvents and chemical shift change for each Ile and Phe residue of FliG$_{MC}$, related to Figure 3,4 and 5. (A) Difference of contacted solvents (top) and chemical shift change (δ; bottom) for each Ile and Phe residue between FliG$_{MC}$ and FliG$_{MC}$-G215A. (B) Difference of contacted solvents (top) and chemical shift change (δ; bottom) for each Ile and Phe residue between FliG$_{MC}$ and FliG$_{MC}$-HP. In the bar plot for difference of contacted solvents, the residues in red and blue depict the increased and decreased number of interacting water molecules in FliG$_{MC}$-G215 or FliG$_{MC}$-HP compared with FliG$_{MC}$, respectively. In the bar plot for the chemical shift change, the δ for each Ile and Phe residue of FliG$_{MC}$ upon G215A mutation (A, bottom) and applying pressure (B, bottom) were calculated by the following equation: $\delta = [(\delta^{1}H)^{2}+0.3\delta^{13}C)^{2}]^{1/2}$ (Blue bar). The $\delta^{1}H$ and $\delta^{13}C$ indicated that chemical shift changes of the ^{1}H and ^{13}C axes of the 2D ^{1}H-^{13}C NMR spectrum, respectively. The red bar indicates the residue whose ^{1}H-^{13}C signal broadening out upon G215A mutation (A, bottom) or applying pressure (B, bottom).

Table S1. **The Difference in solvent accessibility and number of contact solvents among $FliG_{MC}$, $FliG_{MC}$-HP, and $FliG_{MC}$-G215A, related to Figure 5. *** The increase and decrease of each value are shown in red and blue, respectively.

Residue	$FliG_{MC}$-HP vs. $FliG_{MC}$		$FliG_{MC}$-G215A vs. $FliG_{MC}$	
	Diff. No. of contact solvents*	Diff. Accessibility*	Diff. No. of contact solvents*	Diff. Accessibility*
Ile				
ILE:140	0.11	-0.01	-0.43	-0.02
ILE:141	0.46	0.01	0.14	0.00
ILE:148	-0.43	-0.09	-1.78	-0.17
ILE:151	-0.70	-0.04	-1.45	-0.08
ILE:164	-0.40	0.00	-0.62	0.00
ILE:180	-0.62	0.00	0.83	0.01
ILE:197	-3.25	-0.30	-3.25	-0.29
ILE:213	1.26	0.03	0.15	0.10
ILE:222	0.07	0.00	-0.08	0.00
ILE:238	-0.03	0.00	0.28	0.00
ILE:249	0.57	0.00	0.08	0.00
ILE:267	-0.06	0.00	0.63	0.00
ILE:310	0.53	0.01	-0.19	-0.01
ILE:328	0.01	0.00	0.08	0.00
ILE:331	0.84	0.02	0.35	0.02
Phe				
PHE:168	0.64	-0.02	-0.96	-0.03
PHE:202	-0.54	-0.01	0.91	0.03
PHE:254	0.63	-0.01	-0.87	-0.03
PHE:256	1.59	0.08	1.99	0.02
PHE:295	0.31	0.01	0.02	0.01
PHE:350	0.93	0.13	-1.3	-0.12

Table S2. **List of strains and plasmids, related to Flagellar rotation analysis of FliG mutants (STAR★METHODS).**

Rif^r, rifampin resistant; Pof$^+$, normal polar flagellum; Laf$^-$, defective in lateral flagellar formation; Pof$^-$, defective in polar flagellar formation; Mot-, defective in polar flagellar motility; TP^r, trimethoprim resistant; Sm^r, streptomycin resistance; Cm^r, chloramphenicol resistance; P_{tac}, *tac* promotor; P_{lac}, *lac* promotor; Amp^r, Ampicillin resistance.

Strains or plasmids	Genotype or description	Reference or source
V. alginolyticus		
VIO5	Wild type strain of a polar flagellum (Rif$^+$ Pof$^+$ Laf$^-$)	(S1)
NMB198	VIO5Δ*fliG* (Pof$^-$, Mot$^-$)	(S2)
E. coli		
DH5α	F$^-$, Φ80d*lacZ*ΔM15, Δ(*lacZYA-argF*)U169, *deoR*, *recA*1, *endA*1, *hsdR*17(r_K^-, m_K^+), *phoA*, *supE*44, λ$^-$, *thi*-1, *gyrA*96, *relA*1 (Host for cloning experiments)	(S3)
S17-1	*recA hsdR thi pro ara RP-4 2-tc::Mu-Km::Tn7* (Tp^r Sm^r)	(S4)
BL21(DE3)	*F$^-$, ompT, hsdS$_B$*(r_B^- m_B^-), *gal*($\lambda_c I$ 857, *ind1*, *Sam7*, *nin5, lacUV*5-T7*gene*1)*, dcm*(DE3) (Host for protein expression)	Novagen
Plasmids		
pMMB206	Cm^r, $P_{tac}P_{lac}$UV5	(S5)
pNT1	*fliG* in pMMB206	(S6)
pColdI	Cold shock expression vector, Amp^r	TaKaRa
pColdI-FliG$_{MC}$	FliG$_{MC}$ fragment (G122-L351) in pColdI	(S7)

References

S1. I. Okunishi, I. Kawagishi, M. Homma. (1996). Cloning and characterization of motY, a gene coding for a component of the sodium-driven flagellar motor in Vibrio alginolyticus. *J Bacteriol* 178, 2409-2415. 10.1128/jb.178.8.2409-2415.1996

S2. T. Yorimitsu, A. Mimaki, T. Yakushi, M. Homma. (2003). The conserved charged residues of the C-terminal region of FliG, a rotor component of the Na+-driven flagellar motor. *J Mol Biol* 334, 567-583. 10.1016/j.jmb.2003.09.052

S3. S. G. Grant, J. Jessee, F. R. Bloom, D. Hanahan. (1990). Differential plasmid rescue from transgenic mouse DNAs into Escherichia coli methylation-restriction mutants. *Proc Natl Acad Sci U S A* 87, 4645-4649. 10.1073/pnas.87.12.4645

S4. R. Simon, U. Priefer, A. Puhler. (1983). A BROAD HOST RANGE MOBILIZATION SYSTEM FOR INVIVO GENETIC-ENGINEERING - TRANSPOSON MUTAGENESIS IN GRAM-NEGATIVE BACTERIA. *Bio-Technology* 1, 784-791. 10.1038/nbt1183-784

S5. V. M. Morales, A. Bäckman, M. Bagdasarian. (1991). A series of wide-host-range low-copy-number vectors that allow direct screening for recombinants. *Gene* 97, 39-47. 10.1016/0378-1119(91)90007-x

S6. N. Takekawa, S. Kojima, M. Homma. (2014). Contribution of many charged residues at the stator-rotor interface of the Na+-driven flagellar motor to torque generation in Vibrio alginolyticus. *J Bacteriol* 196, 1377-1385. 10.1128/JB.01392-13

S7. Y. Onoue, R. A. Yoshizumi, M. Gohara, Y. Nishino, S. Kobayashi, Y. Asami, M. Homma. (2016). Domain-based biophysical characterization of the structural and thermal stability of FliG, an essential rotor component of the Na +-driven flagellar motor. *Biophys Physicobiol* 13, 227-233. 10.2142/biophysico.13.0_227